Calculated Momentum Distributions and Compton Profiles of Interacting Conduction Electrons in Lithium and Sodium†

B. I. Lundqvist*
Laboratory of Solid State and Atomic Physics, Cornell University, Ithaca, New York 14850

and

C. Lydén
Department of Theoretical Physics, Chalmers University of Technology, Fack, S-402 20 Göteborg, Sweden

(Received 24 March 1971)

The momentum distributions and Compton profiles of the conduction electrons in Li and Na are calculated considering effects of orthogonalization of the core electrons, periodic potential, and correlation. Using the orthogonalized-plane-wave method with parameters from Callaway and electron-gas data from an earlier calculation by Lundqvist, we find that the anisotropy of the Compton profile should be measurable for single crystalline Li but not for Na, and that the results compare well with recent experimental data for polycrystalline Li and Na. There is a slight indication of correlation effects beyond those considered here, but more accurate experimental data are needed for a more decisive conclusion.

I. INTRODUCTION

Electron states in metals are objects for widely ramified studies. Usually the distribution of electrons with respect to energy is pursued, as for instance in photoemission and soft-x-ray emission measurements. However, there are also some experiments related to the distribution of electrons with respect to momentum, as measurements of Compton scattering of x rays[1] and of angular correlation in positron annihilation.[2]

The interpretation of the positron-annihilation experiment is impeded by the need of knowing the positron wave function and the perturbation of the electron states due to the presence of the positron.[3] On the other hand, the Compton scattering experiment performed under proper conditions is to a good approximation directly related to the momentum distribution of occupied states.

In recent years some reasonably accurate measurements of Compton profiles, i.e., distribution of the scattered x rays with respect to the Doppler shift in their wave numbers, have been performed on solids,[4–6] and more accurate measurements are in progress.[7] Thus we feel it well motivated to aim at a detailed comparison between experiment and theory. The purpose of this paper is to present calculations of momentum distributions and Compton profiles for conduction electrons in lithium and sodium to provide a theoretical basis for such a comparison. Effects of electron-electron interactions as well as of the band structure have been considered.

In a model with free and independent electrons the Compton profile is an inverted parabola.[1] Deviations from this simple shape are found experimentally[4–6] and caused by three different effects, which all act to broaden the distribution: (a) The interaction between the electrons ("correlation") pushes a part of the occupied states below the Fermi momentum k_F to momentum values above k_F[8]; (b) in a real metal the conduction electrons have to be excluded from the ionic core region, i.e., the conduction-electron wave function has to be orthogonal to the inner core states,[9] and the rapid spatial variation of the latter requires high momentum components; (c) finally the periodic potential in the pure metal couples electron states in different bands, particularly states close to the Brillouin-zone boundaries. These are all well-known effects, but we illustrate their influence on the shape of the Compton profile by explicit calculations. Lithium and sodium have been chosen for these calculations, because the potential effect (c) is very different in these two metals.

In sodium the lattice potential has a very weak effect on the conduction electrons. We show that the distortion of the Compton profile because of (c) is hardly measurable in sodium. The core-orthogonalization effect (b) is easily accounted for, and so the magnitude of the correlation effect (a) is shown to be detectable from accurate measurements on sodium.

In lithium, on the other hand, the potential effect (c) is the leading one. Because of the strong effective potential, states in the lowest bands are strongly coupled, in particular near the Brillouin-zone boundaries. This means that the electron wave function contains strong high momentum components and that the momentum distribution for

lithium will be very anisotropic. The Compton profiles from measurements in different directions on a single crystal should thus have different shapes. We show that a comparison of these profiles will give important information about both the crystal potential and the electron correlations.

The calculations are performed using recent electron-gas data[10] for the correlation effects and an orthogonalized-plane-wave (OPW) scheme for the band structures.[11] While there are similar studies performed for the angular correlation in positron annihilation in metals,[12] where obviously the correlation effects enter quite differently,[3] to our knowledge only separate estimates of band structure[6,13] and correlation effects[14] on the Compton profiles for conduction electrons have been published earlier.

In Sec. II the relation between the Compton profile and the momentum distribution is established, and the conditions for the experiment briefly discussed. This treatment is a direct generalization of the Platzman-Tzoar electron-gas treatment[15] to inhomogeneous electron systems. Further, an expression for the momentum distribution for conduction electrons in metals is derived, and it is concluded that correlation effects can be considered by using mean occupation numbers calculated for the electron gas. In Sec. III the calculations of correlation and band-structure effects together with the further steps leading to the Compton profiles are described. The results are presented in Sec. III. The paper is concluded with a discussion in Sec. IV.

II. COMPTON SCATTERING AND MOMENTUM DISTRIBUTION

Scattering of x rays by electrons is in the nonrelativistic region properly treated in the Born approximation,[16] where the differential scattering cross section per unit solid angle and unit interval of outgoing energy of the scattered photon is given by[17]

$$\frac{d^2\sigma}{d\Omega\, d\omega} = AS(\vec{k},\omega)\ . \tag{1}$$

In this equation the prefactor A depends on the individual properties of the scattering electrons, i.e., their classical electron radius $r_0 = e^2/m$, and on the frequencies ω_1 and ω_2 and the polarization directions $\hat{e}_1$ and $\hat{e}_2$ of the incoming and outgoing photons, respectively,

$$A = r_0^2(\omega_2/\omega_1)\,(\hat{e}_1\cdot\hat{e}_2)^2\ . \tag{2}$$

We use units in which $\hbar = c = 1$. The dynamical structure factor $S(\vec{k},\omega)$, which should be evaluated for the energy and momentum transfers

$$\omega = \omega_1 - \omega_2\ ,\quad \vec{k} = \vec{k}_1 - \vec{k}_2\ , \tag{3}$$

describes the density fluctuations of all the electrons. Expressed in electron field operators $\psi(\vec{r},t)$,[17-19]

$$S(\vec{k},\omega) = \sum_m \int_{-\infty}^{\infty} \frac{dt}{2\pi}\, e^{i\omega t}\frac{1}{V}\int d^3x_1 \int d^3x_2\, e^{-i\vec{k}\cdot(\vec{x}_1-\vec{x}_2)} \times \langle \psi^+(\vec{x}_1,t)\psi(\vec{x}_1,t)|N,m\rangle\langle N,m\,|\psi^+(\vec{x}_2,0)\psi(\vec{x}_2,0)\rangle\ , \tag{4}$$

where the bracket $\langle\cdots\rangle$ denotes the thermal average for the system of N electrons and V is the volume of the crystal. It is obvious from Eq. (1) that inelastic scattering of x rays in principle can be used to probe the full density-fluctuation spectrum of an electron system.[20] The Compton scattering experiment, however, gives information about a particular limiting form of $S(\vec{k},\omega)$, in the ideal case being performed at x-ray energy transfers ω much higher than the characteristic energies E_B of the system. When this condition is fullfilled the scattering process is too quick to allow more than one electron to be affected by the x-ray photon, and the potential that the electron is moving in may be thought of as a constant.[21] Then the "impulse approximation"[22] is applicable, which means that the intermediate states $|N,m\rangle$ may be assumed to factorize into a state with one energetic free electron and a state with the rest of the system unchanged,

$$|N,m\rangle \simeq |\vec{k}+\vec{p}\rangle\,|N-1,m\rangle\ . \tag{5}$$

Just as for the electron gas[15] we then get

$$\frac{d^2\sigma}{d\Omega\, d\omega} = r_0^2(\hat{e}_1\cdot\hat{e}_2)^2\,\frac{\omega_2}{\omega_1}\int \frac{d^3p}{(2\pi)^3}\,\delta\left(\omega - \frac{k^2}{2m} - \frac{\vec{p}\cdot\vec{k}}{m}\right)N(\vec{p})\ , \tag{6}$$

where $N(\vec{p})$ now is the momentum distribution of a nonhomogeneous system,

$$N(\vec{p}) = \frac{1}{V}\int d^3x_1 \int d^3x_2\, e^{i\vec{p}\cdot(\vec{x}_1-\vec{x}_2)}\langle\psi^\dagger(\vec{x}_1,0)\psi(\vec{x}_2,0)\rangle\ . \tag{7}$$

From Eq. (6) we see that the scattered photon is shifted in frequency both by the recoil energy $E_R = k^2/(2m)$ and the Doppler shift $\vec{p}\cdot\vec{k}/m = -qk/m$. Beside the energy factor ω_2/ω_1, the differential cross section is thus proportional to the Compton profile,

$$J_z(q) = \frac{2V}{N}\int\int_{p_z=|q|} N(\vec{p})\,\frac{dp_x\,dp_y}{(2\pi)^3}\ , \tag{8}$$

where the integration is performed over a plane perpendicular to the direction of the momentum transfer $\vec{k}$.

If the energy transfer ω were not much larger than the characteristic energies of the system, the Compton-scattered electron would end up in a state closely above the Fermi level, being able to exchange and interact strongly with the other electrons and the hole left behind. These processes are not described in the impulse approximation.

Due to the polarization of the remaining conduction electrons the energetic electron acquires two extra contributions to its energy besides the free-electron value $p'^2/(2m)$: an imaginary part, which for large p' goes asymptotically like[23]

$$\mathrm{Im}E_{p'} \to -(\omega_p/2a_0p')\ln(k_cv'/\omega_p)\,, \tag{9}$$

where ω_p is the plasma frequency, k_c is the cut-off momentum for plasma oscillations, and $v'=p'/m$; and a real shift[24]

$$\Delta(\mathrm{Re}E_{p'}) \to -\pi\omega_p/4a_0p'\ . \tag{10}$$

In addition to the condition for the impulse approximation ($E_R \gg E_B$, Ref. 22), Eq. (6) requires that these two contributions (for $\vec{p}'=\vec{p}+\vec{k}$) are negligible compared with $\vec{p}\cdot\vec{k}/m$. This is certainly the case, when the momentum transfer k is much larger than the Fermi momentum k_F.

The common energy-band picture is successful in at least qualitative descriptions of different experimental results and is theoretically meaningful as a first approximation for the description of quasiparticle states.[25] The natural way to calculate the momentum distribution is to first derive an expression for $N(\vec{p})$ by expanding the field operators in Bloch waves,

$$\psi(\vec{x},\,t)=\sum_{\vec{k},\,i} a_{\vec{k},\,i}(t)\,\varphi_{\vec{k},\,i}(\vec{x})\ . \tag{11}$$

The amplitude $a_{\vec{k},\,i}$ can be interpreted as annihilating an electron with wave vector $\vec{k}$ in the band denoted by the reciprocal-lattice vector $\vec{G}_i$. We use here the reduced zone scheme, so that $\vec{k}$ belongs to the first Brillouin zone. Expanding the Bloch waves in plane waves,

$$\begin{aligned} &|\,\varphi_{\vec{k},\,i}\,\rangle=\textstyle\sum_{\vec{G}}\alpha_i(\vec{k}+\vec{G})\,|\,\vec{k}+\vec{G}\,\rangle\,,\\ &\langle\vec{x}\,|\,\vec{k}\,\rangle=e^{i\vec{k}\cdot\vec{x}}/V^{1/2}\,, \end{aligned} \tag{12}$$

we get the momentum distribution as

$$N(\vec{p})=\sum_{i,j}\sum_{\vec{G}}\alpha_i^*(\vec{p})\alpha_j(\vec{p})n_{ij}(\vec{p}-\vec{G})\,, \tag{13}$$

where $\vec{p}-\vec{G}$ is restricted to the first Brillouin zone, and where we have introduced a mean occupation number for Bloch states,

$$n_{ij}(\vec{k})=\langle\,a^{\dagger}_{\vec{k},\,i}(0)a_{\vec{k},\,j}(0)\,\rangle\ . \tag{14}$$

For noninteracting electrons the diagonal occupation numbers $n_{ii}(\vec{k})$ are different from zero only for a part of the lowest band (monovalent metals) where they take the value of 1, and all the nondiagonal numbers are 0. In the interacting case the diagonal noninteger number $n_{ii}(\vec{k})$ gives the mean occupation number of the Bloch state with wave vector $\vec{k}$ in the band $\vec{G}_i$. The nondiagonal numbers are due to mixing between different bands caused by the electron-electron interaction. As shown in the Appendix these numbers give negligible contributions to the momentum distribution, when the nearly-free-electron approximation is applicable. Then we have

$$N(\vec{p})=\sum_{\vec{G}_i,\,\vec{G}}|\,\alpha_i(\vec{p})\,|^2n_{ii}(\vec{p}-\vec{G})\,, \tag{15}$$

where $\vec{p}-\vec{G}$ is in the first Brillouin zone. This is a very accurate expression for sodium. We show in the Appendix that if deviations from it were present for lithium, they should first show up close to the zone boundaries.

In Eq. (15) the effects of the electron-electron interaction enter primarily through the occupation numbers, and the core-orthogonalization and periodicity effects enter primarily through the square of the plane-wave coefficients. In principle both quantities should be calculated for the fully interacting system. Accurate values for the momentum distribution can, however, be obtained by using mean occupation numbers $n(\vec{k})$ calculated for the electron gas and calculating the wave functions for a good effective one-electron potential. The presence of the ions does not change the electron-gas values of $n_{ii}(\vec{k})$ very much. In an accurate effective crystal potential, on the other hand, there have to be some effects of the electron-electron interaction included,[26] either calculated from many-body theory or deduced empirically.

III. CALCULATIONS AND RESULTS

A. Momentum Distributions

The calculations of the momentum distributions $N(\vec{p})$ require according to Eq. (15) information about the occupation numbers $n_{ii}(\vec{p})$ and the plane-wave coefficients $|\,\alpha_i(\vec{p})\,|^2$ of the Bloch states. As discussed in the Appendix the occupation numbers for Bloch states in a free-electron-like metal, except for the anisotropy, are close to the momentum distribution of the electron gas,

$$n(p)=Z_F\Theta(k_F-p)+n_c(p)\,,$$

where Z_F is the magnitude of the step at the Fermi surface, $\Theta(x)$ the unit step function, and $n_c(p)$ the continuous part. We may thus write

$$\begin{aligned} n_{ii}(\vec{p}-\vec{G}') &\simeq n(\vec{p}-\vec{G}'+\vec{G}_i)\\ &=Z_F\Theta[E_F-E(\vec{p}-\vec{G}'+\vec{G}_i)]\\ &\quad+n_c(|\,\vec{p}-\vec{G}'+\vec{G}_i\,|)\,. \end{aligned} \tag{16}$$

Here the condition $E(\vec{k})=E_F$ defines the Fermi sur-

face, $E(\vec{k})$ being the band energy.

The momentum distribution of the electron gas has earlier been calculated by one of the authors[10] in an approximation, which goes beyond the well-known treatment by Daniel and Vosko (DV).[8] The same formal approximation for the electron self-energy has been applied in the two calculations. However, while the DV treatment concerns only the first two terms in an expansion of the electron Green's function,[27] the calculation of Ref. 10 contains an infinite summation. At high metallic densities the deviations between the results are small, typically 0.02–0.03 electron states per spin and momentum volume unit at $r_s = 2$. [The electron-gas parameter is defined by $3/(4\pi r_s^3)$ = electron density.] At lower densities the deviations become significant, and the DV method breaks gradually down.[27]

The self-energy considered in Refs. 8 and 10 is the dynamically screened exchange term, i.e., the lowest-order term in an expansion in the dynamic effective interaction in the conduction-electron medium.[28] An estimate of the next term in such an expansion given by Geldart *et al.*[27] indicates a further decrease in the renormalization constant Z_F.[29]

The approximation of Ref. 10 emphasizes the coupling of electrons to plasmons.[30] The occupied states with $\vec{k}$ outside the Fermi surface can be interpreted as majorly incoherent hole-plasmon states, which require a rather high energy to get excited.[24] In the same way the unoccupied states with $\vec{k}$ below k_F consist of incoherent electron-plasmon pairs.

Applying Eq. (16), we can explicitly write the different kinds of contributions to the momentum distribution as

$$N(\vec{p}) = |\alpha_0(\vec{p})|^2 n(\vec{p}) + \sum_{\vec{G}\neq\vec{0}} |\alpha_0(\vec{p})|^2 n(\vec{p}-\vec{G}) + \sum_{\vec{G}_i=\vec{G}\neq 0} |\alpha_i(\vec{p})|^2 n(\vec{p}) + \sum_{\vec{G}_i\neq 0,\vec{G}\neq\vec{G}_i} |\alpha_i(\vec{p})|^2 \times n(\vec{p}-\vec{G}+\vec{G}_i), \quad (17)$$

where $\vec{p}-\vec{G}$ is in the first Brillouin zone and $i=0$ denotes the lowest band. In the one-electron approximation only the first two terms of this expression contribute, $n(\vec{p})$ being the step function $\Theta(E_F - E(\vec{p}))$.[12] For a free-electron metal, on the other hand, only the first and third term contribute, as in this case the only nonzero amplitudes are $|\alpha_i(\vec{p})|^2 = 1$, when $\vec{p}-\vec{G}_i$ belongs to the first Brillouin zone. Going over to the extended zone scheme we obtain the familiar electron-gas result.[15] We understand from this that the contribution from the first and third term is almost isotropic, while the second and to a less extent the fourth term represent the major anisotropy in the momentum distribution.

In Fig. 1 we compare the linear momentum distributions for Na and Li, calculated for an electron gas of appropriate density, with those derived by Phillips and Weiss[4] from their measured Compton profiles for polycrystalline samples. For sodium the electron-gas curve falls essentially within the assigned error limits, while there are significant deviations for lithium. To appreciate the difference between these two metals it is convenient to apply the OPW method.

The Bloch functions can alternatively be expressed in OPW's,[31]

$$|\varphi_{\vec{k},i}\rangle = \sum_{\vec{G}} \alpha_i'(\vec{k}+\vec{G}) |\mathrm{OPW}, \vec{k}+\vec{G}\rangle . \quad (18)$$

The transformation into the plane-wave representation is given by

$$\alpha_i(\vec{k}+\vec{G}) = \alpha_i'(\vec{k}+\vec{G}) - \sum_{\vec{G}'} \langle \vec{k}+\vec{G}|\mathcal{P}|\vec{k}+\vec{G}'\rangle \alpha_i'(\vec{k}+\vec{G}') , \quad (19)$$

where $\mathcal{P}$ is the projection operator onto the core states.

The strong periodic potential for the conduction electrons in lithium makes the momentum distribution $N(\vec{p})$ of this metal anisotropic, and one has to perform a full band calculation to obtain $N(\vec{p})$. We have used an OPW method with the input parameters for lattice potential and core wave function taken from Callaway,[11] i.e., using the Seitz potential.[32]

In the calculations of α and α' [Eqs. (12), (18), and (19)] we have included 19 reciprocal-lattice vectors in the summations. The OPW coefficients $\alpha_i'(\vec{p})$ have been computed in 25 points along each of 18 rays within one irreducible zone. Interpolation between the calculated values for the square of the plane-wave coefficient $\alpha_0(\vec{p})$ has been performed, using an expansion with six cubic harmonics.[33]

The plane-wave coefficient $\alpha_0(\vec{p})$ is shown in Fig. 2 for $\vec{p}$ in the main crystallographic directions. At the zone boundary $\alpha_0(\vec{p})$ changes sign. This is a direct consequence of the fact that our OPW calculation with the Seitz potential gives a rather large and positive value for the effective pseudopotential V_{110} at the reciprocal-lattice vectors $\vec{G}$ of length $(2\pi/a)\sqrt{2}$. In Fig. 3 contours of $|\alpha_0(\vec{p})|^2$ are shown for a plane perpendicular to the $\langle 001\rangle$ direction.

The Fermi momenta are calculated for different directions by solving the equation $E_F = E(\vec{k})$. We have used the expression for $E(\vec{k})$ given in Ref. 12 but a different value for the Fermi energy, $E_F = -0.416$ Ry. This value is the result with 19 OPW's, the number used here and in Ref. 12, while the value $E_F = -0.427$ Ry is calculated with 43 OPW's.[11]

As the mean occupation numbers $n_{ii}(\vec{k})$ fall off very fast for $\vec{k}$ outside the Fermi surface (Fig. 4),

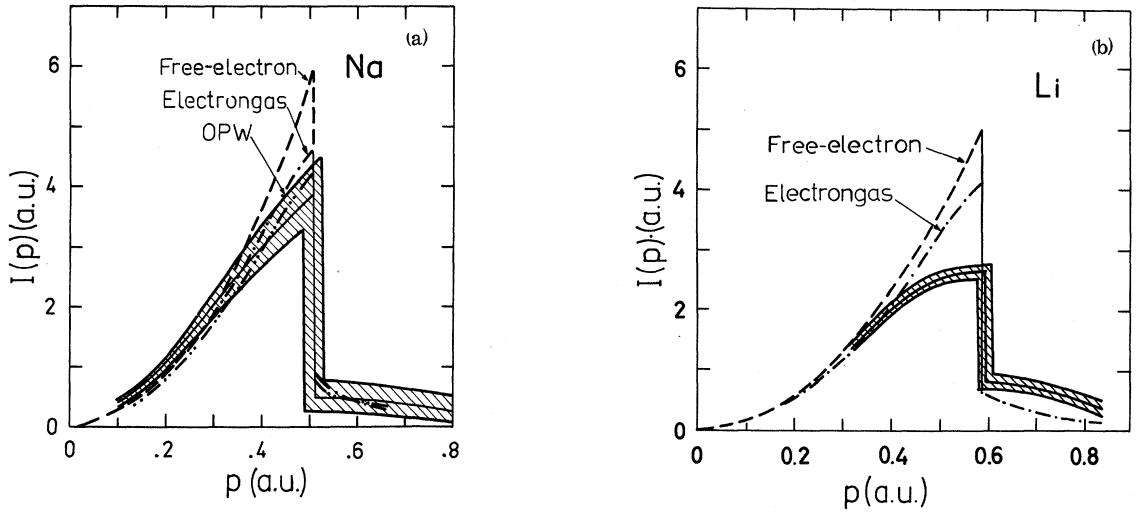

FIG. 1. Momentum densities for conduction electrons in (a) sodium and (b) lithium. The cross-hatched areas are deduced from measured Compton profiles considering the experimental errors (Ref. 4). The curves are the results calculated in the free-electron approximation ($3p^2/k_F^3$ for p smaller than k_F, 0 elsewhere) and from electron-gas data (Ref. 10). In (a) the result in the one-OPW approximation (see text) is drawn too.

the momentum distribution $N(\vec{p})$ can be obtained with sufficient accuracy including only a few terms in Eq. (17). In the summations over bands we have only considered the reciprocal-lattice vectors having lengths 0 or $(2\pi/a)\sqrt{2}$ and further made the sufficiently accurate replacements $\alpha_i(\vec{p}) \simeq \alpha_0(\vec{p}-\vec{G}_i)$ for $\vec{p}-\vec{G}_i$ in the first Brillouin zone and $\alpha_i(\vec{p}) \simeq -\alpha_0(\vec{p}+\vec{G}_i)$ for $\vec{p}-\vec{G}_i$ outside the first zone.

The first term in Eq. (17) gives the main contribution. The second term has a maximum of about 0.2 for momenta around $0.74\times(1/\sqrt{2},\ 1/\sqrt{2},\ 0)$ a.u., while the third and fourth terms contribute less than 0.02 at any momentum, the fourth being of interest only close to the zone boundaries $\vec{p}\cdot\vec{G} = \vec{G}^2$, where $\vec{G}$ is any of the twelve reciprocal-lattice vectors of length $(2\pi/a)\sqrt{2}$.

The momentum distribution $N(\vec{p})$ for Li calculated from Eqs. (16), (17), and (19) is shown for the three main crystallographic directions in Fig. 5. The anisotropy is significant. For example, the reduction from the free-electron values just below

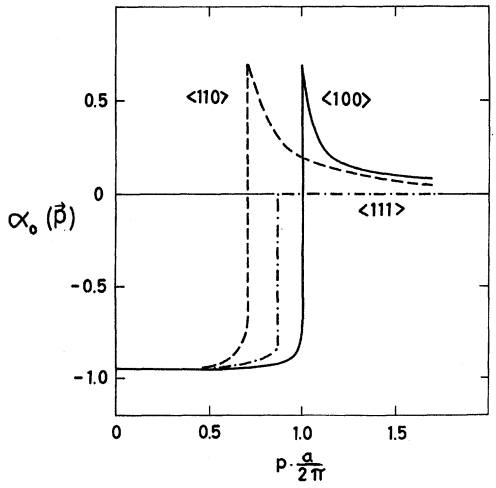

FIG. 2. Plane-wave coefficient $\alpha_0(\vec{p})$ for the lowest-energy band in lithium in the main crystallographic directions.

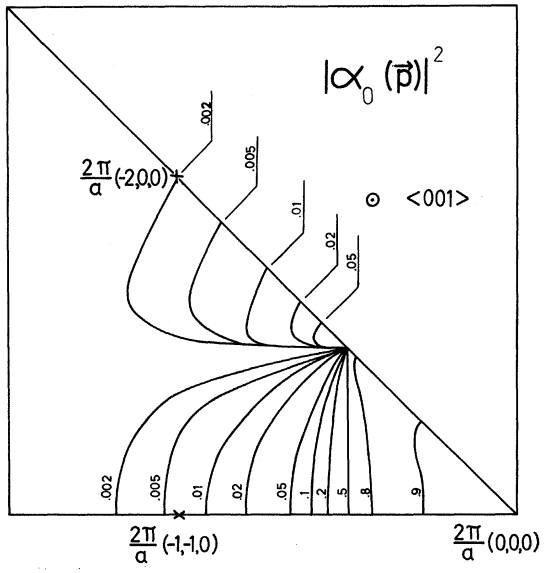

FIG. 3. Contours of the squared plane-wave coefficient $|\alpha_0(\vec{p})|^2$ for the lowest band and for momenta in a plane perpendicular to the ⟨001⟩ direction in lithium.

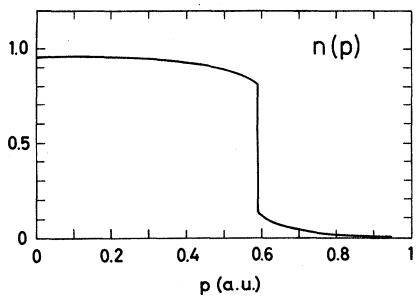

FIG. 4. Momentum distribution $n(p)$ for an electron gas with the same density as the conduction electrons in lithium ($r_s = 3.2$).

the Fermi surface is equal to 0.27, 0.40, and 0.29 in the ⟨100⟩, ⟨110⟩, and ⟨111⟩ directions, respectively, as compared to the calculated electron-gas value 0.19 at the Li conduction-electron density ($r_s = 3.2$). The Fermi momenta are 0.574, 0.605, and 0.580 a.u. for the same directions. The bump at higher p values in the ⟨110⟩ direction originates from the second term in Eq. (17), $G_{110} - k_F$ being 0.74 a.u.

In sodium the effective lattice potential is much weaker than in lithium. The pseudopotential V_{110} is about 0.03 Ry, for Na[34] as compared with about 0.12 Ry for Li.[11] Such a weak interband coupling makes the pseudo-wave-function plane-wave-like for states away from the zone boundary. If we neglect the interband coupling completely, which amounts to putting only the OPW coefficients $\alpha_i'(\vec{p})$ for $\vec{p} - \vec{G}_i$ in the first Brillouin zone different from zero, we get from Eq. (19)

$$\alpha_{\vec{G}_i}(\vec{k}+\vec{G}) = (\delta_{\vec{G},\vec{G}_i} - \langle \vec{k}+\vec{G}|\mathcal{P}|\vec{k}+\vec{G}_i\rangle)/(1 - \langle \vec{k}+\vec{G}_i|\mathcal{P}|\vec{k}+\vec{G}_i\rangle)^{1/2} \ . \quad (20)$$

Using Herman-Skillman atomic wave functions[35] in the evaluation of this expression we estimate

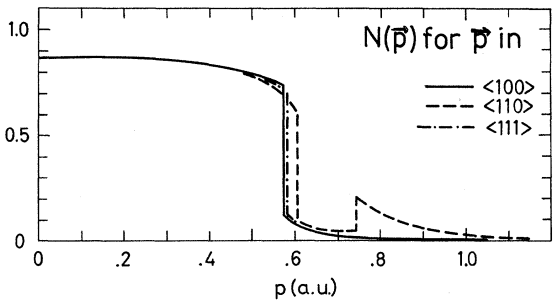

FIG. 5. Calculated momentum distribution $N(\vec{p})$ for Li along three directions in a single crystal. Effects of both electron-electron interaction and of band structure are included.

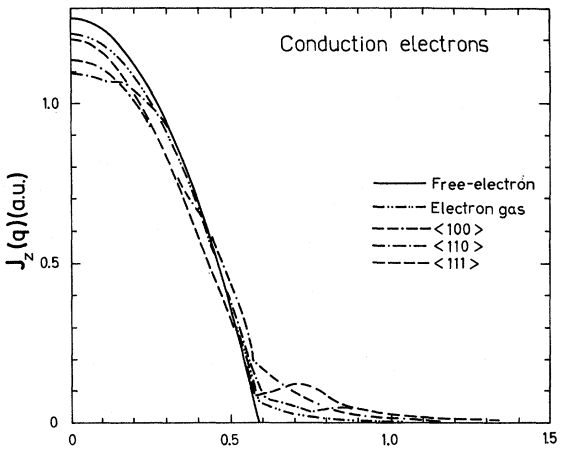

FIG. 6. Calculated Compton profiles $J_z(q)$ for free noninteracting electrons and for interacting conduction electrons in lithium for three orientations of a single crystal. The profile for an electron gas with the lithium conduction-electron density ($r_s = 3.2$) is also shown.

$|\alpha_i(\vec{p})|^2$ to be 0.93, constant inside the first Brillouin zone. The second term of Eq. (17) is according to Eq. (19) smaller than 0.006 and is negligible, as is the fourth term. In the one-OPW approximation we thus get an isotropic momentum distribution $N(\vec{p})$, 7% lower than the electron-gas values at momenta within the first Brillouin zone. The result is shown as the lower Na curve in Fig. 1. The slight enhancement for higher momenta required by the normalization of $N(\vec{p})$ will raise the latter curve above the correlation curve for momenta larger than about 0.6 a.u.

The anisotropy of $N(\vec{p})$ comes about in two ways: The shape of the Fermi surface determines the location of the discontinuities in the momentum distribution, and the coupling to higher bands determines the redistribution to higher momentum components. The Fermi surface is known to be spherical within 1%.[36] We estimate the contribution from the second and fourth terms of Eq. (17) using degenerate perturbation theory in the pseudopotential V_{110} on a two-band model. Compared with the one-OPW result we get a slight reduction in $N(\vec{p})$ for p below k_F, amounting to at most 3% just below k_F in the ⟨110⟩ direction. The step at $p = G_{110} - k_F$ is 0.03, as compared to 0.16 for Li in the same kind of approximate treatment.[37] From this we conclude that the anisotropy is substantially smaller in Na than in Li, and that it is doubtful, whether it is measurable.

B. Compton Profiles

The Compton profiles calculated from Eq. (8) for the conduction electrons in lithium are shown in Fig. 6 for the three crystal directions, together with the

profiles for free noninteracting electrons [$N(\vec{p}) = \Theta(k_F - p)$] and for the interacting electron gas. The two-dimensional integral in Eq. (8) has been computed numerically with interpolations for $|\alpha_i(\vec{p})|^2$ and $n(\vec{p})$ in Eq. (17).

The major anisotropy of the Compton profile, caused by the second term in Eq. (17), depends on how many Fermi "spheres" the plane $p_z = q$ penetrates in the repeated zone scheme.[38] The effect of the periodicity on the shape of the Compton profile is most pronounced in the center and for momenta outside the Fermi surface. The difference in height at $q = 0$, the $\langle 111 \rangle$ curve being about 10% higher than the $\langle 110 \rangle$ curve and 5% higher than the $\langle 100 \rangle$ curve, is mainly due to the fact that in the integration planes perpendicular to the $\langle 111 \rangle$, $\langle 100 \rangle$, and $\langle 110 \rangle$ directions there are six, four, and two nearest-neighboring zones, respectively. When the integration plane $p_z = q$ moves in the z direction, other sets of nearest neighbors give contributions, and such contributions become dominant for q outside the Fermi surface. For instance, in the $\langle 111 \rangle$ direction and for q at about 0.8 a.u. a pronounced peak appears due to contributions from the zones around the reciprocal-lattice vectors $\vec{G}a/(2\pi) = (1, 1, 0)$, $(1, 0, 1)$, and $(0, 1, 1)$.

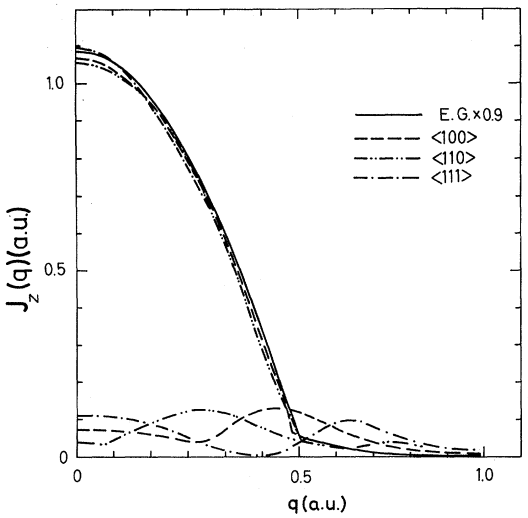

FIG. 8. Same curves as in Fig. 6 with the high momentum contributions [second and fourth terms in Eq. (17)] subtracted. The contribution from the high momentum plane-wave coefficients is shown in the lower part of the figure. Further, the electron-gas curve (E.G.) multiplied with $|\alpha_0(0)|^2 = 0.9$ is shown.

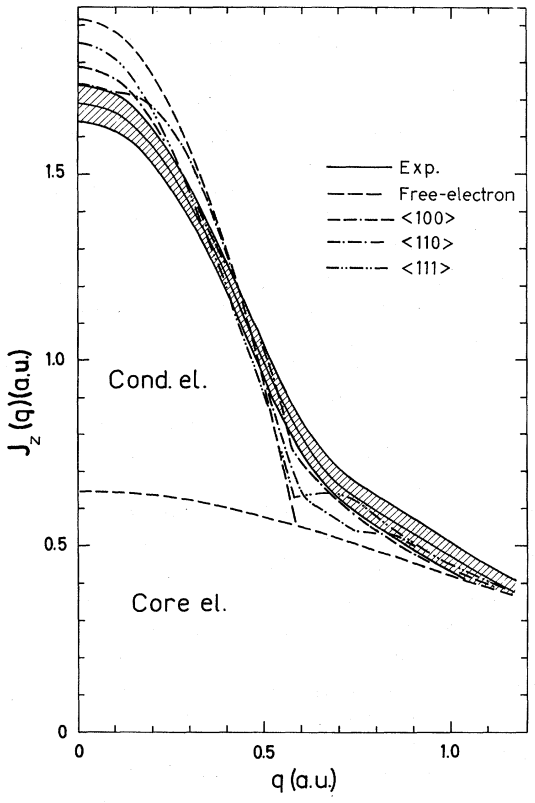

FIG. 7. Calculated Compton profiles for lithium in Fig. 6 are added to the cross section for the core electrons (Ref. 41). The experimental Compton profile (EXP) for polycrystalline Li with background subtracted and with the experimental uncertainty indicated (Refs. 4 and 42) is shown for comparison.

The calculated Compton profiles shown in Fig. 6 saturate the sum rule

$$\int_{-\infty}^{\infty} J_z(q)\, dq = 1 \quad \text{per electron} \tag{21}$$

within 0.5%. We estimate the numerical errors in the curves to be considerably less than 1% of the value at $q = 0$.

In Fig. 7 our calculated profiles are compared with the experimental results measured on polycrystalline Li by Weiss and Phillips.[4] An estimate of the cross section for the core electrons, calculated in the impulse approximation from atomic Hartree-Fock wave functions,[39] has been added to our curves for the conduction electrons. The area under the core-electron curve is 1.98 times the area under the free-electron curve, as the integrated Compton intensity is $1 - f^2(\sin\theta_c/\lambda_1)$ per electron, where f is the x-ray scattering factor, $2\theta_c$ the Compton scattering angle, and λ_1 the incident wavelength. The experimental curve is multiplied with ω_1/ω_2 to compensate for the factor ω_2/ω_1 in (6). Further it is folded around $q = 0$ and averaged. The error bars allow for the asymmetry in the core-electron contribution due to departure from the result of the impulse approximation.[40] We normalize the experimental curve by equalizing the area under it, with the background subtracted, to the area under the core + free-electron curve.

As the momentum distribution of sodium is iso-

tropic to a high degree, the common analysis for isotropic systems[41] is applicable. Then to a good approximation, the linear momentum distribution $I(p)$ according to Eqs. (8) and (17) satisfies

$$\frac{I(p)}{(4\pi p^2)} = |\alpha_0(p)|^2 n(p) = \frac{2\pi^2 N}{V} \left| \frac{dJ_z(q)}{q\,dq} \right|_{q=p} . \qquad (22)$$

This relation has been used by Weiss and Phillips in deducing the curves in Fig. 1 from the experimental Compton profiles.[4]

IV. DISCUSSION AND CONCLUSIONS

We have shown that effects due to correlation, core orthogonalization, and periodic potential introduce significant deviations from the free-electron results for the momentum distributions and the Compton profiles of conduction electrons in metals. Accordingly, accurate measurements of the Compton scattering should give valuable information on electron-electron interaction, wave functions, and band structure of these electrons. Here we first discuss the agreement between our results and existing experimental data, then we analyze the possibility of isolating the three effects, and finally we draw some tentative conclusions about calculations of effects of electron-electron interaction.

For sodium, the linear momentum distribution, calculated with correlation and core-orthogonalization effects included, is within the range of the experimental uncertainty,[4] as shown in Fig. 1. The improvement compared with the free-electron result is obviously significant and predominantly due to the electron-electron interaction.

For lithium the calculated anisotropic profiles, Fig. 7, fall close to the measured result for polycrystalline material, considering the uncertainty assigned to the data by Phillips and Weiss[4] and Weiss.[40] Our calculations are thus able to account for the major part of the deviations from the free-electron behavior in both Na and Li.

Figure 7 also shows that our calculation predicts the anisotropy to be measurable. This result does not contradict the findings in Ref. 4 that the Compton profile from a Li single crystal within the experimental uncertainty has no deviation from spherical symmetry. As can be seen from Fig. 7, the shaded region indicating this uncertainty is broad enough to contain the spread between the three extremal directions. Use of nonstandard x-ray equipment should increase the accuracy considerably,[4] thus making variations such as the ones in the calculated curves detectable.

For lithium there are several evidences of a large value V_{110} of the effective periodic potential. Angular correlation measurements in positron annihilation indicate a highly anisotropic Fermi surface.[42] Band calculations, using different constructions of the lattice potential, all give a large and positive V_{110},[11,37,43-46] the Seitz potential giving V_{110}[11] roughly 10 to 15% higher than potentials based on the Gáspár-Kohn-Sham or Slater expressions for exchange[45] or on the quantum defect method.[43] Assuming the core wave function and the potential to be known, it should be possible to investigate effects from the electron-electron interaction also in lithium. The main anisotropic contributions to the momentum distribution come from the second and fourth terms in Eq. (17). This is illustrated in Fig. 8, where the calculated Compton profiles for Li are separated into two contributions, one from the first and third terms in Eq. (17) and one from the second and fourth terms. In Fig. 8 we further show a Compton profile derived from an isotropic momentum distribution $N(p) = |\alpha_0(0)|^2 n(p)$, i.e., the same expression as that used for sodium. The contributions to the Compton profiles from the first and third terms in Eq. (17) are seen to fall very close to this curve. From this we can see a possible way to analyze experimental data: (i) Measure the Compton profiles for the main directions of a single crystal, (ii) adjust the crystal potential to make the contributions from the second and fourth terms of Eq. (17) conform with the measured anisotropies, (iii) subtract this contribution, and (iv) apply the analysis used for Na earlier to the remaining essentially isotropic profile.

The Compton-profile measurement is a very promising technique to investigate the effects of the electron-electron interaction in a variety of electron systems. Recent experiments[47] on liquid and gaseous helium have to a high accuracy shown that the wave function of He is known very well, indirectly verifying the validity of the impulse approximation in the limit $E_B \ll E_R$ (Ref. 22). Experimental results for liquid and gaseous H_2 show not only the effects of binding very clearly but also deviations from the calculated profiles, which have been attributed to non-Hartree-Fock electron-electron interaction.[47] With deviations for such a simple system as H_2 one might of course wonder whether effects can be treated at all in metals. However, there exist treatments of the electron-electron interaction, which go beyond the Hartree-Fock approximation, as for instance the one used in our calculation. The question is, how well the present approximation works?

In sodium the potential and core effects are fairly well known. Band calculations show a very weak effective periodic potential,[34,43] and several experiments support the view of an almost spherical Fermi surface.[36] The one OPW curve in Fig. 1, which includes effects of correlation, is within the experimental range. On the other hand, out of the experimental data we can extract a value of the electron-gas Fermi discontinuity Z_F in the

range 0.5–0.75, large enough to include the results of both Refs. 10 and 27. Furthermore, using a Fermi-momentum value k_F calculated from x-ray data for the lattice parameter[48] rather than the value found by Weiss and Phillips,[4] the one-OPW curve in Fig. 1 is pushed outside the experimental range for some regions of p values.

The experimental Compton profiles for lithium[4] are slightly broader than the calculated ones, Fig. 7. As the primary source for such a broadening we suggest some higher-order electron-electron interaction effects, since we believe the core-orthogonalization and potential effects to be rather accurately considered.

Thus from the present comparison of our result with the available experimental data we recognize a slight indication that effects of the electron-electron interaction, beyond those considered here, might be present. To make such a conclusion definite, however, more accurate measurements have to be done together with an analysis along the lines suggested above.

ACKNOWLEDGMENT

One of the authors (B. I. L.) gratefully acknowledges a travelling grant from Letterstedtska Resestipendiefonden.

APPENDIX: MEAN OCCUPATION NUMBER

In this appendix we will estimate the effects of the presence of the ions on the mean occupation number n_{ij} [Eq. (14)]. We will do so in the approximation, where the interactions between the electrons are considered to the lowest order in the dynamically screened interaction. This approximation is discussed at length by Hedin and Lundqvist (HL) in Ref. 25, and frequent references to this article will be made. We will estimate the effect of the Bloch wave coupling in the nearly-free-electron (NFE) approximation.

The mean occupation number can be expressed as an energy integral of the electron Green's function G_{ij},

$$n_{ij}(\vec{k}) = (1/\pi)\int_{-\infty}^{\mu} d\epsilon\, \mathrm{Im} G_{ij}(\vec{k},\epsilon)\ , \tag{A1}$$

where

$$G_{ij}(\vec{k},\epsilon) = [\epsilon - \underline{E}(\vec{k}) - \underline{\Sigma}(\vec{k},\epsilon)]^{-1}_{ij}\ , \tag{A2}$$

and where $\vec{k}$ is in the first Brillouin zone. For noninteracting electrons, G_{ij} and n_{ij} are diagonal. Nondiagonal elements can arise from self-energy effects, expressed by Σ_{ij}, that is from the interaction of the electron with the medium of electrons, which in turn reacts back on the electron.

The coupling between an individual electron and the density fluctuations of the medium, $\rho(\vec{r}) = \Sigma_q \rho_q e^{i\vec{q}\cdot\vec{r}}$, is expressed by matrix elements of the type

$$\langle \varphi_i(\vec{k}) | e^{i\vec{q}\cdot\vec{r}} | \varphi_j(\vec{k}') \rangle\ .$$

In a homogeneous electron gas φ_i and φ_j are plane-wave states, and the matrix element gives the selection rule $\vec{k}-\vec{k}'=\vec{q}$, which leads to a diagonal Green's function. In a crystalline solid φ_i and φ_j are Bloch wave states, and due to the periodic potential there are nonzero matrix elements also for $\vec{k}-\vec{k}'=\vec{q}+\vec{K}$, where $\vec{K}$ is a reciprocal-lattice vector. A quantity suitable to measure the deviations from homogeneity in a periodic system is [Eq. (34.14) of Ref. 25]

$$\Delta(\vec{k},\vec{q};\vec{K}) = \int_V d^3r\, \varphi^*_{\vec{k}+\vec{q}+\vec{K}}(\vec{r})\, e^{i\vec{q}\cdot\vec{r}}\, \varphi_{\vec{k}}(\vec{r}) - \delta_{\vec{K},0}\ , \tag{A3}$$

where now the Bloch states are characterized by their wave vectors in the extended zone scheme. It appears in umklapp and nondiagonal terms of the dielectric function [Eq. (34.13) of Ref. 25] and of the electron self-energy [Eq. (35.4) of Ref. 25]. This formulation of the problem is useful, when the Bloch wave coupling Δ is a small quantity.

The major effect of the nonhomogeneity on the diagonal elements of the self-energy is accounted for by replacing the Coulomb potential $v(\vec{q})$ in the expression for $\Sigma_{jj}(\vec{k},\epsilon)$ by $v(\vec{q})|1+\Delta(\vec{k},\vec{q};0)|^2$ [Eq. (35.3) of Ref. 25]. The nondiagonal elements of the self-energy are to the lowest order in Δ [Eq. (35.4) of Ref. 25]

$$\Sigma_{i0}(\vec{k},\epsilon) = \frac{i}{(2\pi)^4}\int d^3q\, d\omega \left(\frac{W(\vec{q},\omega)\Delta(\vec{k},\vec{q};\vec{K}_i)}{\omega+\epsilon - E(\vec{k}+\vec{q}+\vec{K}_i)} + \frac{W(\vec{q},\omega)\Delta^*(\vec{k}+\vec{K}_i,\vec{q};-\vec{K}_i)}{\omega+\epsilon - E(\vec{k}+\vec{q})} \right)\ , \tag{A4}$$

where $W(\vec{q},\omega)$ is the dynamically screened electron interaction with local field effects neglected, and $i=0$ indicates the lowest-energy band.

There is no explicit evaluation of the coupling function $\Delta(\vec{k},\vec{q};\vec{K})$ available in the literature. Different crude estimates of the function in different limits indicate that its effects are usually small (HL, Sec. 34),[49,50] both in the umklapp contributions to the diagonal part of the dielectric constant in the weak-binding limit,[49] and in the umklapp contributions to the diagonal part of the self-energy in aluminum.[50]

We will briefly discuss the effects of the periodic potential on the mean occupation number $n_{ij}(\vec{k})$ in the NFE approximation. When expressed in the supposedly small parameter

$$\beta_{\vec{k}}(\vec{K}) = V_{\vec{K}}/[E(\vec{k}+\vec{K}) - E(\vec{k})]\ ,$$

where $V_{\vec{K}}$ is a Fourier component of the effective periodic potential, the coupling $\Delta(\vec{k},\vec{q};0)$ is small to order β^2, and according to perturbation theory

$$\Delta(\vec{k},\vec{q};\vec{K}) \simeq \beta_{\vec{k}}(\vec{K}) - \beta_{\vec{k}+\vec{q}}(\vec{K})\ , \tag{A5}$$

when $\vec{K}$ is different from zero. This interband coupling function is thus small except close to the zone boundaries, i.e., where $\beta_{\vec{k}}(\vec{K})$ or $\beta_{\vec{k}+\vec{q}}(\vec{K})$ are large, in which case degenerate perturbation theory has to be used. For $\vec{k}$ off the zone boundary the region where Δ is appreciable is just a small fraction of the whole $\vec{q}$ space, which is integrated over in Eq. (A4). This implies that the nondiagonal matrix element in Eq. (A4) is much smaller than $\Sigma_{00}(\vec{k}, \epsilon)$ and $\Sigma_{ii}(\vec{k}, \epsilon)$.

We will now estimate the nondiagonal element of the mean occupation number n_{i0} for the case, when the nondiagonal elements of $\underline{\Sigma}$ are much smaller than the diagonal ones. We limit ourselves to the practically interesting case, when $\vec{K}_i$ is one of the reciprocal-lattice vectors having length $(2\pi/a)\sqrt{2}$. To lowest order in the interband coupling

$$G_{i0} \simeq G_{ii}\Sigma_{i0}G_{00} . \tag{A6}$$

The imaginary part of this expression contains only one term of importance for energies $\epsilon(<\mu)$ of interest in Eq. (A1),

$$n_{i0}(\vec{k}) \approx (1/\pi)\int_{-\infty}^{\mu} d\epsilon\, \mathrm{Im}G_{00}(\vec{k}, \epsilon)\, \mathrm{Re}\Sigma_{i0}(\vec{k}, \epsilon)\, \mathrm{Re}G_{ii}(\vec{k}, \epsilon) , \tag{A7}$$

and in this integral the major contribution comes from the quasiparticle energy branch $\epsilon = E(\vec{k})$, where $\mathrm{Im}G_{00}$ is sharply peaked. On the other hand, $\mathrm{Im}G_{ii}(\vec{k}, \epsilon)$ is very small for $\epsilon < \mu$, as it is describing the unlikely event of a combined creation of a hole with wave vector $\vec{k} - \vec{K}_i$ and electron-hole (or plasmon) excitations. This together with the smallness of the nondiagonal elements Σ_{i0} and the fact that the structure of $\mathrm{Re}G_{00}(\vec{k}, \epsilon)$ does not contribute to an integral like (A1) are the reasons why only the term in Eq. (A7) needs to be considered.

Using expressions for noninteracting electrons in this estimate, Eq. (A7) becomes

$$n_{i0}(\vec{k}) \simeq \mathrm{Re}\Sigma_{i0}[\vec{k}, E(\vec{k})]/[E(\vec{k}) - E(\vec{k} - \vec{K}_i)] . \tag{A8}$$

The largest value of n_{i0} is obtained at the Fermi surface in the direction of $\vec{K}_i$. The diagonal part of the self-energy, $\mathrm{Re}\Sigma_{00}[\vec{k}, E(\vec{k})]$, has a weak $\vec{k}$ dependence, and in the alkali metals its magnitude is about twice the magnitude of the vertical energy gap $E(\vec{k}_F) - E(\vec{k}_F - \vec{K}_i)$.[51] We conclude from this that $n_{i0}(\vec{k})/n_{00}(\vec{k})$ is small, once

$$\mathrm{Re}\Sigma_{i0}[\vec{k}, E(\vec{k})]/\mathrm{Re}\Sigma_{00}[\vec{k}, E(\vec{k})]$$

is so. Thus the nondiagonal elements $n_{i0}(\vec{k})$ of the mean occupation number are much smaller than the diagonal ones $n_{00}(\vec{k})$ for NFE metals, where the effective potential $V_{\vec{K}}$ is much smaller than the vertical energy difference, i.e., $\beta_{\vec{k}}(\vec{K})$ is small.

In the same way we see that the diagonal elements $\Sigma_{jj}(\vec{k}, \epsilon)$ of the self-energy in the NFE metals are close to the self-energy for the electron gas. As we use a representation in the Bloch states of the lattice, any anisotropy in the electron energies $E_i(\vec{k})$ will also be reflected in $n_{ii}(\vec{k})$, as indicated in Eq. (16).

Sodium is certainly free-electron-like, as $\beta_{\vec{k}}(\vec{K}_i)$ is smaller than about 0.1 everywhere in the occupied part of the band. Further, the core-orthogonalization effects on Δ are small in Na.[52] For lithium the NFE treatment is valid in the bottom of the conduction band, $\beta_0(\vec{K}_i)$ being about 0.06, but as $\vec{k}$ approaches the zone boundary, $\beta_{\vec{k}}(\vec{K}_i)$ grows larger, and the conclusion on the smallness of $n_{i0}(\vec{k})$ is then less well founded. In principle $\Delta(\vec{k}, \vec{q}; \vec{K})$ could be calculated with, e.g., the OPW method applied earlier in this paper, but due to its strong dependence on $\vec{k}$, $\vec{q}$, and $\vec{K}$, the explicit computation of the self-energy matrix would be an extensive task, beyond the scope of the present paper. We content ourselves to notice that, if present, the effects of the nondiagonal parts of the mean occupation number should be most pronounced in the neighborhood of the zone boundaries defined by $2\vec{k}\cdot\vec{K}_i - \vec{K}_i^2 = 0$, i.e., in the same region, where the distortion of the energy bands is largest.

In the NFE approximation, the plane-wave coefficients $\alpha_i(\vec{k}+\vec{G})$ are proportional to $\beta_{\vec{k}+\vec{G}_i}(\vec{G}-\vec{G}_i)$ for $\vec{G} \neq \vec{G}_i$. In the expression for the momentum distribution $N(\vec{p})$ [Eq. (13)] the nondiagonal terms then are small to at least order β^2 and thus completely negligible for NFE metals.

The problem with the nondiagonal occupation numbers can in principle be eliminated by choosing a better Bloch wave representation in Eq. (13). A completely diagonal representation of the momentum distribution should be given by the eigenfunctions of the first-order density matrix, the Löwdin natural spin orbitals.[53,54] However, in practice it is very difficult to find these orbitals without previous knowledge of the wave function.[55]

---

†Work partially supported by the Swedish Natural Science Research Council and by a grant from the Xerox Corp.

*On leave from Department of Theoretical Physics, Chalmers University of Technology, Göteborg, Sweden.

[1]A. H. Compton and S. K. Allison, *X Rays in Theory and Experiment*, 2nd ed. (Van Nostrand, Princeton, N.J., 1967).

[2]See, e.g., *Positron Annihilation, Proceedings of the Conference Held at Wayne University*, 1965, edited by A. T. Stewart and L. O. Roellig (Academic, New York, 1967).

[3]J. P. Carbotte and S. Kahana, Phys. Rev. 139, A213 (1965).

[4]W. C. Phillips and R. J. Weiss, Phys. Rev. 171, 790 (1968).

[5]M. Cooper, J. A. Leake, and R. J. Weiss, Phil. Mag.

12, 797 (1965); M. Cooper and J. A. Leake, *ibid.* 15, 1201 (1967); R. J. Weiss and W. C. Phillips, Phys. Rev. 176, 900 (1968); Phil. Mag. 20, 1239 (1969); W. C. Phillips and R. J. Weiss, Phys. Rev. 182, 923 (1969); R. J. Weiss, Phys. Rev. Letters 24, 883 (1970); Phil. Mag. 21, 1169 (1970); T. Fukamachi and S. J. Hosoya, J. Phys. Soc. Japan 28, 161 (1970); S. Manninen and O. Inkinen, Phys. Scripta 1, 186 (1970); R. Currat, P. D. DeCicco, and R. Kaplow, Phys. Rev. B 3, 243 (1971).

[6]M. Cooper, B. G. Williams, R. E. Borland, and J. R. A. Cooper, Phil. Mag. 22, 441 (1970).

[7]P. Eisenberger, Electronic Density of States Symposium, National Bureau of Standards, Gaithersburg, Md., 1969 (unpublished).

[8]E. Daniel and S. H. Vosko, Phys. Rev. 120, 2041 (1960).

[9]C. Herring, Phys. Rev. 57, 1169 (1940).

[10]B. I. Lundqvist, Physik Kondensierten Materie 7, 117 (1968).

[11]J. Callaway, Phys. Rev. 109, 1541 (1958); 124, 1824 (1961); 131, 2839 (1963).

[12]J. Melngailis and S. DeBenedetti, Phys. Rev. 145, 400 (1966).

[13]B. Donovan and N. H. March, Proc. Roy. Soc. (London) 69, 1249 (1956).

[14]G. E. Kilby, Proc. Phys. Soc. (London) 82, 900 (1963).

[15]P. M. Platzman and N. Tzoar, Phys. Rev. 139, A410 (1965).

[16]I. Waller and D. R. Hartree, Proc. Roy. Soc. (London) A124, 119 (1929).

[17]L. van Hove, Phys. Rev. 95, 249 (1954).

[18]M. N. Rosenbluth and N. Rostocker, Phys. Fluids 5, 776 (1962).

[19]D. F. DuBois and V. Gilinsky, Phys. Rev. 133, A1308 (1964).

[20]V. Ohmura and N. Matsudaira, J. Phys. Soc. Japan 19, 1355 (1964); Y. Mizuno and Y. Ohmura, *ibid.* 22, 445 (1967).

[21]P. Eisenberger and P. M. Platzman. Phys. Rev. A 2, 415 (1970).

[22]C. F. Chew and G. C. Wick, Phys. Rev. 85, 636 (1952).

[23]J. J. Quinn, Phys. Rev. 126, 1453 (1962).

[24]B. I. Lundqvist, Physik Kondensierten Materie 6, 193 (1967); Phys. Status Solidi 32, 273 (1969).

[25]L. Hedin and S. Lundqvist, in *Solid State Physics*, edited by H. Ehrenreich, F. Seitz, and D. Turnbull (Academic, New York, 1970), Vol. 23, p. 1, hereafter denoted by HL.

[26]See, e.g., Ref. 25, Sec. 35.

[27]D. J. W. Geldart, A. Houghton, and S. H. Vosko, Can. J. Phys. 42, 1938 (1964).

[28]See, e.g., Ref. 25, Sec. 25.

[29]See Fig. 26 in Ref. 25 for a comparison.

[30]B. I. Lundqvist, Physik Kondensierten Materie 6, 206 (1967).

[31]See, e.g., W. A. Harrison, *Pseudo-Potentials in the Theory of Metals* (Benjamin, New York, 1966).

[32]F. Seitz, Phys. Rev. 47, 400 (1935).

[33]F. C. von der Lage and H. A. Bethe, Phys. Rev. 71, 612 (1947).

[34]A. J. Hughes and J. Callaway, Phys. Rev. 136, A1390 (1964); 137, AB4 (1965).

[35]F. Herman and S. Skillman, *Atomic Structure Calculations* (Prentice-Hall, Englewood Cliffs, N.J., 1963).

[36]M. J. G. Lee, Phys. Rev. 178, 953 (1969).

[37]As shown by Ham and Kenney, (see Ref. 43) the two-band model is inaccurate in reproducing the band structure of Li and Na. However, for semiquantitative estimates, of the kind done here, it is applicable.

[38]See, e.g., Fig. 5 of Ref. 12.

[39]R. J. Weiss, A. Harvey, and W. C. Phillips, Phil. Mag. 17, 241 (1968).

[40]R. J. Weiss (private communication).

[41]W. E. Duncanson and C. A. Coulson, Proc. Phys. Soc. (London) 57, 190 (1945).

[42]J. J. Donaghy and A. T. Stewart, Phys. Rev. 164, 391 (1967).

[43]F. Ham, Phys. Rev. 128, 82 (1962); 128, 2524 (1962); J. F. Kenney, Solid State and Molecular Theory Group, MIT Quarterly Progress Report, No. 53, 1967 (unpublished).

[44]E. Brown and J. A. Krumhansel, Phys. Rev. 109, 30 (1958).

[45]W. E. Rudge, Phys. Rev. 181, 1033 (1969).

[46]Cf. also Fig. 57 in the review article by M. L. Cohen and V. Heine, in *Solid State Physics*, edited by H. Ehrenreich, F. Seitz, and D. Turnbull (Academic, New York, 1970), Vol. 24, p. 37.

[47]P. Eisenberger, Phys. Rev. A 2, 1678 (1970).

[48]G. W. Pearson, *Handbook of Lattice Spacings and Structures of Metals and Alloys* (Oxford U.P., Oxford, England, 1964), Vol. 4.

[49]N. Wiser, Phys. Rev. 129, 62 (1963).

[50]S. L. Adler, Phys. Rev. 130, 1654 (1963); 141, 814 (1966).

[51]L. Hedin, Phys. Rev. 139, A796 (1965).

[52]L. Hedin, A. Johansson, B. I. Lundqvist, S. Lundqvist, and V. Samathiyakanit, Arkiv Physik 39, 97 (1969).

[53]P.-O. Löwdin, Phys. Rev. 97, 1474 (1955).

[54]O. Goscinskii and P. Linder, J. Math. Phys. 11, 1313 (1970).

[55]A. J. Coleman, Rev. Mod. Phys. 35, 668 (1963).